Cubatic liquid-crystalline behavior in a system of hard cuboids

Bettina S. John, Abraham Stroock, and Fernando A. Escobedo[a)]
School of Chemical and Biomolecular Engineering, Cornell University, Ithaca, New York 14853-5201

(Received 2 February 2004; accepted 27 February 2004)

The lyotropic phase behavior of cuboidal particles was investigated via Monte Carlo simulations. Hard cubes were approximated by suitably shaped clusters of hard spheres. Changes in concentration and structure of the system were monitored as a function of osmotic pressure P^* (imposed in an isobaric ensemble). As expected, an isotropic phase prevailed at low concentrations (low P^*) and a crystalline phase formed at high concentrations (high P^*). A third distinct phase was also observed for an intermediate range of concentrations (approximately marked by breaks in the P^* versus concentration curve). The structure of this mesophase was characterized both visually and analytically by calculating radial distribution functions and order parameters. It was found that such a mesophase exhibits orientational ordering along three axes (cubatic order) but significant translational disorder, thus having a structure clearly distinct from both isotropic and crystalline phases. © *2004 American Institute of Physics.* [DOI: 10.1063/1.1711594]

I. INTRODUCTION

Computer simulations have been widely used in the study of the phase behavior of the colloidal particles of various shapes. Theoretical and simulation studies of many model systems have predicted rich and intriguing phase behavior,[1] though some of the novel phases predicted have yet to be observed experimentally. Examples of such novel but *unobserved* phases include the biaxial liquid-crystalline phase where two of the particle axes are aligned, the cubatic liquid-crystalline phase where three of the particle axes which are equivalent are aligned, the cubatic phase where particles assemble in short stacks that are mutually perpendicular, and the multinematic phases where more than two ordered phases coexist.[1]

Systems of particles with as varied geometry as spherocylinders, platelets, cut spheres, cylinders, and ellipsoids have been investigated in detail using simulations, particularly in the athermal hardcore limit where all attractive interparticle interactions are screened out. The interest in particles of such geometries ensues from the fact that many colloidal particles are nonspherical. For instance, some clay particles are platelet like, red blood cells are toroidal, and Tobacco Mosaic Virus, inorganic V_2O_5 particles, and boehmite needles are rod shaped.[2] The existence of liquid-crystalline phases is critically dependent on the aspect ratio and geometry of the particles as only sufficiently nonspherical particles can exhibit lyotropic phase transitions.[3,4]

Nanoparticles have been widely used in photography, catalysis, biological labeling, photonics, optoelectronics, information storage, surface-enhanced Raman scattering, and formation of magnetic ferrofluids.[5] The shape of the nanoparticle is of key importance for such applications. Nanoparticles with a large surface area to volume ratio have potential applications in many areas including catalysis and nanocomposites. Particles with unconventional shapes have been recently synthesized which may exhibit interesting and as-yet uncharted liquid-crystalline phase behavior. For example, Sun and Xia have recently synthesized gold and silver nanocubes.[5] They observed that some of the nanocubes self-assembled on a silicon substrate. Cubes, with their symmetry along three axes, are good candidates to explore liquid-crystalline phase behavior. In this work we investigate the bulk phase behavior of cubical particles using Monte Carlo simulations.

Simulation studies have served to establish the existence of entropy-driven liquid-crystalline transitions—that is, transitions where the participating particles experience purely repulsive interactions. In such systems, the isotropic fluid becomes unstable (with respect to an ordered phase) at sufficiently high concentrations because the loss of orientational entropy is compensated by the increase in packing entropy associated with the ordered phase. In the following, we briefly review some of the key findings regarding the liquid-crystalline behavior of spherocylinders, ellipsoids, platelets, cutspheres, and cylinders. For concreteness, only lyotropic transitions are considered.

Stroobants *et al.*[6] simulated hard parallel spherocylinders and detected the presence of nematic and smectic phases. Bolhuis and Frenkel[7] mapped out the phase diagram of hard spherocylinders as a function of aspect ratio. Besides the isotropic and nematic phases, a smectic and two crystalline phases, *AAA* stacked and *ABC* stacked phases, were detected. Camp and Allen[8] mapped out the phase behavior of hard ellipsoids as a function of aspect ratio. Four homogeneous fluid phases were detected: Namely, an isotropic phase, nematic phase (where the long molecular axes of the molecules are aligned parallel to each other), discotic phase (where the short molecular axes of the molecules are aligned parallel to each other), and biaxial phase (with all molecular symmetry axes having their own preferred directions of alignment). Consistent with experimental observations, it

a)Author to whom correspondence should be addressed. Electronic mail: fe13@cornell.edu

was found that the introduction of a small degree of biaxiality weakens the isotropic–nematic transition.

Eppenga and Frenkel[9] simulated the phase behavior of infinitely thin hard platelets. They found a weak first-order isotropic–nematic transition in the limit of $L/D \to 0$, where L is the thickness and D the diameter of the platelet. More recently, Bates and Frenkel[10] simulated a system of hard cylinders in the ''thin disk'' limit of $L/D \to 0$ and found a nematic–columnar transition that would be first order for aspect ratios $0 < L/D \leqslant 0.1$. Veerman and Frenkel[11] studied particles shaped as cut spheres and found that the phase behavior strongly depended on the aspect ratio L/D. For $L/D = 0.1$, isotropic, nematic, columnar, and solid phases were observed. For $L/D = 0.2$, besides the phases listed above, a cubatic phase with cubic orientational order but no translational order was observed. This cubatic phase, wherein the cut spheres stack up in short columns which are perpendicular to one another, has not been experimentally observed thus far. Since the cut spheres with $L/D = 0.2$ assembled in columns of four to five particles that resembled cylinders with $L/D \sim 1.0$, systems of cylinders were thought to be good candidates to observe a cubatic phase.[12] However, simulations of cylinders of aspect ratio $L/D = 0.9$ did not reveal a cubatic phase; instead, another ordered phase (in addition to a crystal phase) was observed wherein the orientations of the particles were either along a column or perpendicular to it.[12]

The cubatic phase has also been theoretically predicted in at least a couple of studies. Frenkel[13] predicted the existence of a cubatic phase in a system of particles comprising of three perpendicular rods, while Blaak and Mulder[14] predicted a cubatic phase in a system of cross like particles (''Onsager crosses'') when the rods were of approximately equal lengths. The latter authors used a bifurcation analysis and a Gaussian approximation for the nematic orientational distribution function.

As indicated earlier, the purpose of this work is to investigate the bulk phase behavior of hard cuboidal particles in a continuum space. While simulation studies exist on mixtures of on-lattice hard cubes[15] and parallel hard cubes,[16] to the best of our knowledge, there has not been any previous theoretical, simulation, or experimental study of the phase behavior of cubes in an unconstrained free space. Our simulations reveal that in addition to the expected isotropic and crystalline phases, a *cubatic* liquid-crystalline phase is observed where the particles retain translational mobility but the axes of the cubes are aligned parallel to three mutually orthogonal directors. This *cubatic* phase differs from that found in cut spheres[11] wherein each particle aligns with only one of the three directors. It also differs from a biaxial phase wherein the (three orthogonal) directors are not equivalent. Our simulation results are expected to be complementary to ongoing experimental efforts involving the preparation and characterization of cubic-particle colloidal suspensions.

II. SIMULATION METHODOLOGY

The cuboidal particles were modeled as clusters of tangent hard spheres fitted in a cubical frame. Each such cuboid had three spheres per side, having a total of 26 spheres, leaving its center hollow for computational simplicity. In such a model cuboid, the faces appear to be *rough* and the edges to be dull (see Fig. 1). The number of spheres needed to form a hollow cubical framework with n spheres per side ($n \geqslant 2$) can be shown to be $6n^2 - 12n + 8$. The cuboids are rigid bodies with fixed distances between the constituent spheres and fixed angles among the spheres. This multisite model of a cube was chosen mainly for computational reasons as it allows a simple means to check for cube overlaps; also, the rounded edges of these cuboids can be seen as approximating the dull edges of cubical particles realizable in experiments.[5] Such multisite particles interact with one another only through the hard-sphere excluded volume effects (no depletion-induced attractive interactions are considered). Because the solvent interactions are not simulated explicitly, the model adopted is consistent with an implicit good solvent.

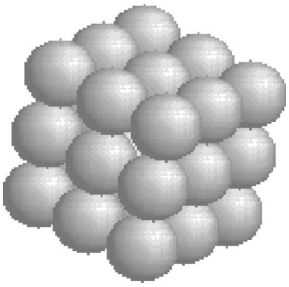

FIG. 1. Model of the cuboid used in the simulation; it has three tangent hard spheres per side with a hollow center.

Most simulation results are reported for a system of $N = 512$ cuboids, with a few selected results for $N = 400$ cuboids. Additional simulations were performed on systems with $N = 64$, 216, and 1584 cuboids to examine finite-size effects. With the exception of the $N = 400$ and $N = 1584$, the value of N was chosen to be $N = i^3$ where i is an integer number to allow the cuboidal particles to close pack in a cubic lattice in a cubic simulation box. Conventional periodic boundary conditions were used to emulate a bulk system. The system was simulated in a continuum space at constant N and constant osmotic pressure P^*. To sample the configurational space for this ensemble, the cuboids were repositioned and reoriented by translation and rigid rotation moves, respectively, while the system density (or concentration) was equilibrated via volume moves.[18] All these moves were accepted by employing the usual Metropolis criterion. In the volume moves, the orientation of each cuboid was kept fixed while the position of its center of mass was rescaled according to the change in the size of the box. Volume changes were isotropic at low pressures; i.e., the box was compressed or expanded equally in all directions, thus retaining the original cubical shape. In contrast, volume moves were anisotropic at high pressures (where ordered structures form); i.e., the box was compressed or expanded to different extents along the three axes independently to allow the box to adopt a geometry that best fit the internal structure. The anisotropic volume moves distort the perfect cubical shape of the box and are only indicated when an ordered structure exist that provides a restoring force against arbitrary box deformations. One Monte Carlo (MC) cycle was comprised of as many translational and rotational moves as the number

of particles in the system and one volume change move. The system of 512 cuboids took at least 10^6 MC cycles to equilibrate at any given pressure.

For the compression runs, the cuboids were initially placed randomly in a cubic box at a very low density. The system was then gradually compressed and equilibrated at each pressure step until it approached the close-packed density. For the expansion runs, the cuboids were initially placed in regular lattice positions (corresponding to the expected cubic crystal structure) at a near close-packed density. The system was then equilibrated at gradually lower pressures until it reached isotropic fluid states. The concentration of particles is reported using the number density $\rho = N/V$, where N is the number of cuboids and V is the volume of the box in a^3 units where a is the minimum distance between two cuboids constrained to slide on a flat surface, which in our case is $a = 2.91\sigma$, where σ is the sphere diameter. Since $\rho = 1$ approximately corresponds to a close-packed system, ρ can also be interpreted as an *effective* packing fraction. While the absolute minimal distance possible between the centers of mass of two cuboids is $a' = 2.798\sigma$, it is impossible to close pack them such that the distance between all nearest-neighbor pairs is a' (unlike the case with a). The dimensionless osmotic pressure reported is $P^* = Pa^3/\varepsilon$, where ε is an arbitrary energy parameter.

The approximate location of the phase boundaries was obtained from the P^* versus ρ curve by detecting discontinuities or changes in slope of such a curve. This approach, which has been widely used before to locate other liquid-crystalline transitions, was found to be convenient for the isotropic–cubatic phase transition as only a small amount of hysteresis was observed between the compression and expansion runs. While free energy calculations could be used to locate phase transitions,[17] they would be very laborious for our system and were not performed here.

The structure of the phases was characterized by using the radial distribution function for the centres of mass of the cuboids (to examine translational order) and order parameters (to measure orientational order). The order parameters adopted here are those used to characterize uniaxial nematic and biaxial order. The use of a biaxial order parameter to characterize order in our system is justified because of the equivalence (symmetry) of the three axes in a cubic particle. If ($\mathbf{x}$,$\mathbf{y}$,$\mathbf{z}$) denote the particle axes (with $\mathbf{z}$ being the most aligned of them) and ($\mathbf{X}$,$\mathbf{Y}$,$\mathbf{Z}$) denote the laboratory axes wherein $\mathbf{Z}$ is the director vector, then the uniaxial order parameter measures the alignment of $\mathbf{z}$ (of all particles) with $\mathbf{Z}$ and the biaxial order parameter measures the alignment of $\mathbf{x}$ and $\mathbf{y}$ (of all particles) with $\mathbf{X}$ and $\mathbf{Y}$, respectively. The ($\mathbf{X}$,$\mathbf{Y}$,$\mathbf{Z}$) vectors were found using a procedure similar to that described in Refs. 8 and 18 as follows. The three axes of one of the cuboids were first taken as reference and each of the three particle axes for all the other cuboids was grouped with one reference axis based on the best alignment. Let the set of unit vectors in each of these three groups be denoted by $\{\mathbf{u}_i\}$, $\{\mathbf{v}_i\}$, and $\{\mathbf{w}_i\}$ (where $i = 1,2,...,N$). For each such set, an ordering tensor was formed, e.g., for $\{\mathbf{u}_i\}$:

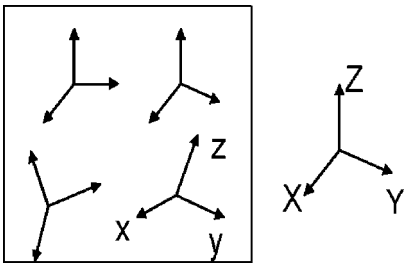

FIG. 2. Schematic of the laboratory axes denoted by X, Y, and Z and the particle axes (inside the box) denoted by x, y, and z. The director vectors (X,Y,Z) of the system for the order parameter calculations are determined such that alignment of particle axes is maximized for the entire system.

$$Q^{uu}_{\alpha\beta} = N^{-1}\sum_{i=1}^{N}\left(\frac{3}{2}u_{i\alpha}u_{i\beta} - \frac{1}{2}\delta_{\alpha\beta}\right), \quad \text{with} \quad \alpha,\beta = 1,2,3,$$

where δ is the Kronecker delta; similar definitions apply for $Q^{vv}_{\alpha\beta}$ and $Q^{ww}_{\alpha\beta}$. The maximum eigenvalues λ^u_+, λ^v_+, and λ^w_+ and their corresponding eigenvectors were found for each of these three ordering tensors $\mathbf{Q}^{uu}$, $\mathbf{Q}^{vv}$, and $\mathbf{Q}^{ww}$. The largest among $(\lambda^u_+, \lambda^v_+, \lambda^w_+)$ identifies the z particle axis (e.g., if λ^u_+ was the largest, then $\{\mathbf{z}_i\} = \{\mathbf{u}_i\}$) and the corresponding eigenvector identifies the laboratory $\mathbf{Z}$ axis. Likewise, the second largest λ_+ and its eigenvector identify the set of y particle axes and the $\mathbf{Y}$ axis, respectively. The remaining set was taken to be the x molecular axis and $\mathbf{X}$ constructed perpendicular to $\mathbf{Z}$ and $\mathbf{Y}$. This idea is illustrated in Fig. 2. Given the equivalence of the cuboid axes, we use an average order parameter to represent the uniaxial order according to

$$Q^2_{00} = 1/3(\langle \mathbf{Z}\cdot\mathbf{Q}^{zz}\cdot\mathbf{Z}\rangle + \langle \mathbf{X}\cdot\mathbf{Q}^{xx}\cdot\mathbf{X}\rangle + \langle \mathbf{Y}\cdot\mathbf{Q}^{yy}\cdot\mathbf{Y}\rangle),$$

while the biaxial order parameter is found from

$$Q^2_{22} = 1/3\langle P(\mathbf{X}\cdot\mathbf{Q}^{xx}\cdot\mathbf{X} + \mathbf{Y}\cdot\mathbf{Q}^{yy}\cdot\mathbf{Y} - \mathbf{X}\cdot\mathbf{Q}^{yy}\cdot\mathbf{X} - \mathbf{Y}\cdot\mathbf{Q}^{xx}\cdot\mathbf{Y}\rangle.$$

In a perfectly aligned biaxial phase where all three particle axes are aligned, $Q^2_{00} = 1$ and $Q^2_{22} = 1$ (Refs. 8 and 18).

III. RESULTS

The equations of state from the compression and expansion runs are shown in Fig. 3. Both curves exhibit three *branches* which can be associated with distinct phases: a low-ρ phase, an intermediate-ρ or mesophase, and a high-ρ phase. The transitions between these phases appear as *breaks* in the curve. The low-ρ and mesophase branches from the expansion and compression curves overlap very well but the high-ρ branch from the compression curve is significantly shifted to the left of the expansion curve. At $P^* \approx 9.9$, a discontinuity (i.e., a jump in density) is observed in both curves, which is indicative of a first-order phase transition between the low-ρ and the mesophase branches. At $P^* \approx 24.6$, a small discontinuity is observed in the expansion curve, but not in the compression curve where only a change in slope is detected; because of this inconsistency, the character of this transition could not be established reliably. This is a reflection of the nonergodic configurational sampling in

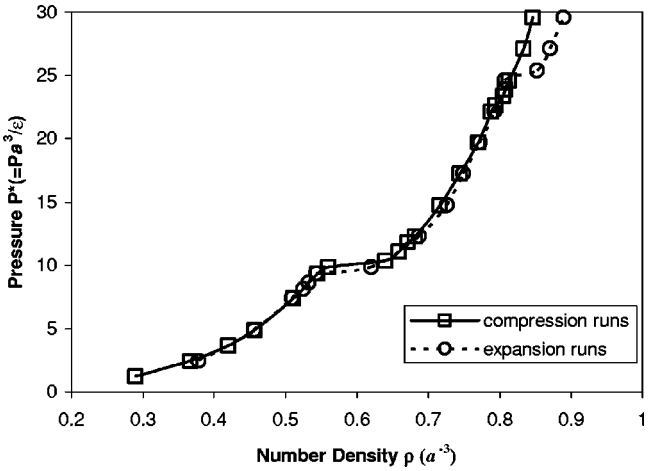

FIG. 3. Simulated equation of state curves for hard cuboids ($N=512$) from the compression runs (squares) and the expansion runs (circles). $P^*=Pa^3/\varepsilon$ where a is a measure of the contact distance between two nearest-neighbor cuboids: $a=2.91\sigma$, where σ is the sphere diameter. Lines are drawn to guide the eye. For $P^*<20$, the error bars are commensurate to but smaller than the data symbols.

the crystal phase which makes unreliable any prediction of the onset and equation of state for the crystal phase.

Figure 4 shows sample snapshots of the system from the compression runs corresponding to $P^*=9.9$ from the low-ρ branch, $P^*=10.3$ and 24.6 from the mesophase branch, and $P^*=29.6$ from the high-ρ branch. Figure 5 shows sample snapshots of the system from the expansion runs corresponding to $P^*=9.4$ from the low-ρ branch, $P^*=9.9$ and 24.6 from the mesophase, and $P^*=29.6$ from the high-ρ branch. The snapshots reveal that the three equation-of-state branches correspond to an isotropic phase (low ρ), a liquid-crystalline phase (mesophase), and a crystalline phase (high ρ), respectively. The mesophase, which exhibits order along

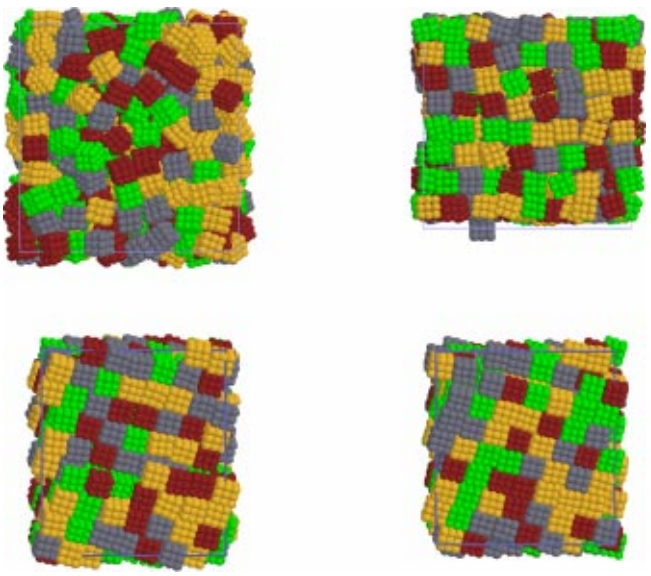

FIG. 4. Snapshots of the system of hard cuboids ($N=512$) from the compression runs for the isotropic phase at $P^*=9.86$ (top left), the cubatic phase at $P^*=10.35$ (top right) and $P^*=24.64$ (bottom left), and the crystalline phase at $P^*=29.57$ (bottom right). The different shades (or colors in the online issue only) are used to better distinguish individual cuboids.

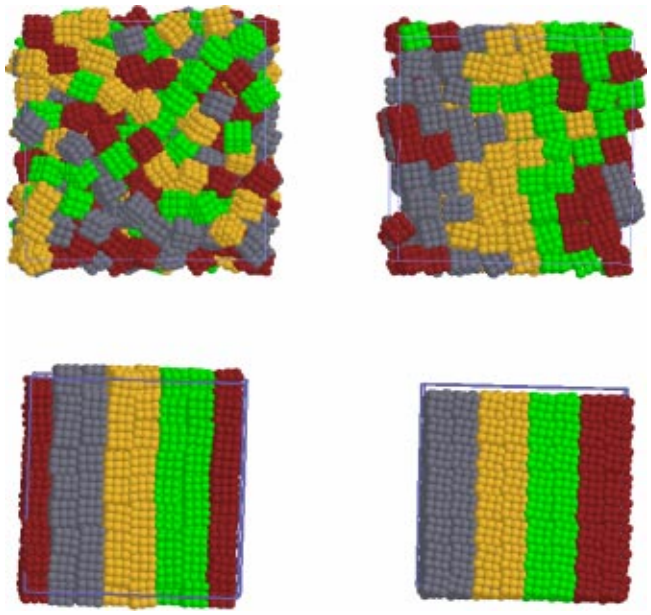

FIG. 5. Snapshots of the system of hard cuboids ($N=512$) from the expansion runs for the isotropic phase at $P^*=9.36$ (top left), the cubatic phase at $P^*=9.86$ (top right) and $P^*=24.64$ (bottom left), and the crystalline phase at $P^*=29.57$ (bottom right). The shades (or colors in the online issue only) are used to better distinguish individual cuboids.

three axes but significant translational disorder, will be subsequently referred to as the cubatic phase. The isotropic–cubatic phase transition then takes place at $P^*=9.9$ and the cubatic–crystal phase transition takes place at around $P^*=24.6$.

In Fig. 5, the changes in the ''banded'' coloring of the cuboids in the initial crystal phase help illustrate the translational mobility (and disorder) of the particles; e.g., by the time the system gets to the cubatic phase at $P^*=9.9$, the bands have completely disappeared. Conversely, in the compression runs in Fig. 4, the translational order in the cubatic phase increases gradually with density, to eventually become a highly layered, crystal-like structure. It can also be seen in the snapshots for the cubatic and crystalline phases that the cuboids are well aligned with the simulation box axes in the expansion runs (Fig. 5), but not so in the compression runs (Fig. 4) where cuboid layers are clearly slanted. Comparing the $P^*=29.57$ snapshots from the compression and expansion routes, it is clear that the structure of the corresponding crystalline phase is different.

The radial distribution function for the centers of mass of the cuboids, $g(r)$, is plotted in Fig. 6 for all three phases as obtained from the compression runs. The $g(r)$ for $P^*=9.9$ (from the low-ρ branch) is typical of an isotropic fluid while that for $P^*=29.6$ (from the high-ρ branch) is typical of a crystalline solid. The $g(r)$ curves for the cubatic phase ($P^*=10.3$ and 24.6) differ from the former two in that a gradual development of long-range translational order occurs. The presence of dual peaks and shoulders in the $g(r)$ of such a phase is indicative of the formation of ordered layers. The exact transition point to the crystalline phase is not discernible from the radial distribution function plots at different pressures. The $g(r)$ plots for the expansion runs are simi-

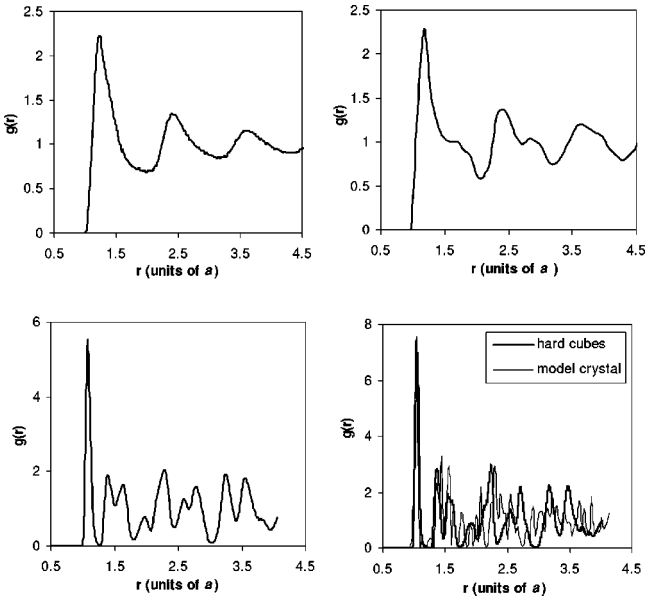

FIG. 6. Radial distribution function for the $N=512$ hard-cuboid system from the compression runs at $P^*=9.86$ (top left, isotropic phase), 10.35 (top right, cubatic phase), 24.64 (bottom left, cubatic phase), and 29.57 (bottom right, crystalline phase). The $g(r)$ at $P^*=29.57$ is compared to that of a model crystal (dotted lines).

lar to those shown in Fig. 6 for the isotropic and cubatic phases but not for the crystal phase. The $g(r)$ for an expansion-run crystal at $P^*=29.6$ is plotted in Fig. 7 where it is shown to agree to a large extent with that of a perfect cubic crystal. The $g(r)$ from a compression-run crystal at $P^*=29.57$ (in the rightmost frame in Fig. 6) does not agree well the perfect crystal $g(r)$ but is shown to agree well with a *model* cubic crystal $g(r)$. To create such a model crystal, the cuboids were first positioned at regular cubic-lattice

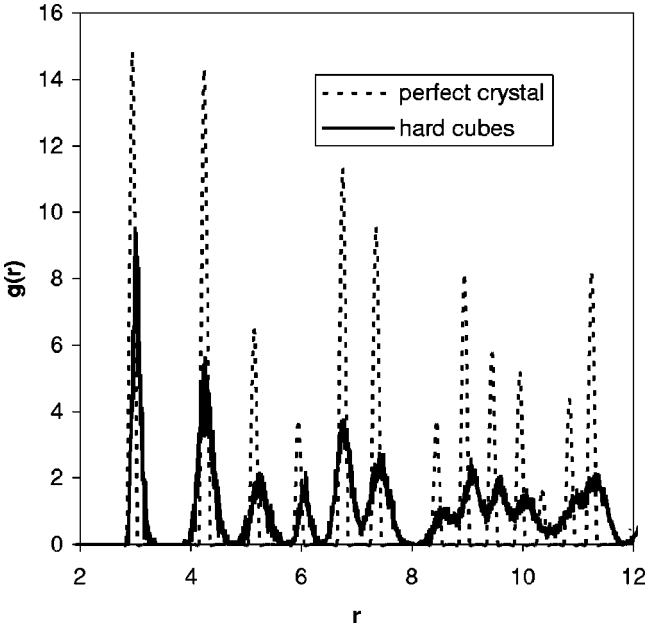

FIG. 7. Radial distribution function for the $N=512$ hard-cuboid system at $P^*=29.57$ (crystalline phase) from the expansion runs (solid lines) and for a perfect cubic crystal at the same density (dotted lines).

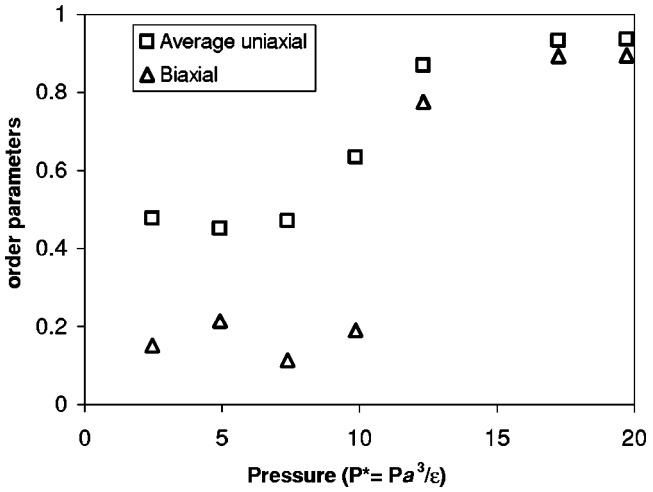

FIG. 8. Average uniaxial order parameter Q_{00}^2 and biaxial order parameter Q_{22}^2 plotted as a function of P^* for systems from the compression runs. The error bars are smaller than the data symbols.

points and then shifted off slightly to resemble the staircase layering observed in simulations. The $g(r)$'s of both model and compression-run crystals have double and shouldered peaks while those of the *perfect* and expansion-run crystals have well-defined single peaks. Such differences in crystal assembly can be attributed to the cuboid surface roughness and reflect two ways of packing of the *bumps* of one cuboid face into the *grooves* of another.

Figures 8 and 9 show the calculated uniaxial and biaxial order parameters for the systems obtained in the compression and expansion runs, respectively. In both figures, these order parameters show: a sharp increase at the isotropic–cubatic phase transition (at $P^*\sim 10$ and immediately after it). Note that the grouping of cuboid axes used to determine the laboratory axes gives rise to an artificially large value for the uniaxial order in the isotropic phase. Note also that the cubatic configurations from the expansion runs have larger order parameters than those from the compression runs; while this difference may reflect some actual structural differences

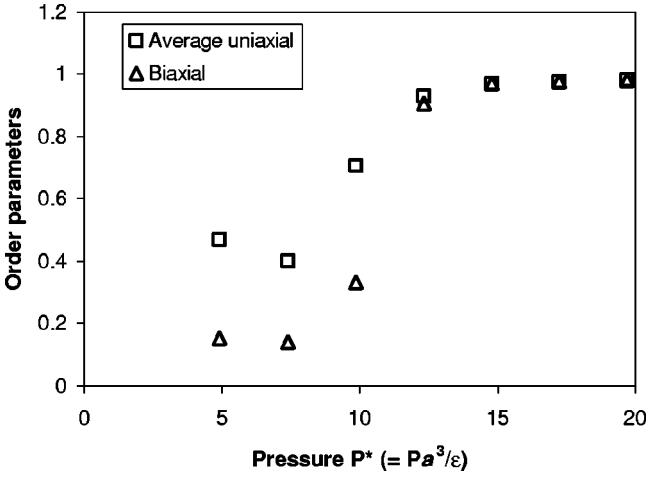

FIG. 9. Average uniaxial order parameter Q_{00}^2 and biaxial order parameter Q_{22}^2 plotted as functions of P^* for systems from the expansion runs. The error bars are smaller than the data symbols.

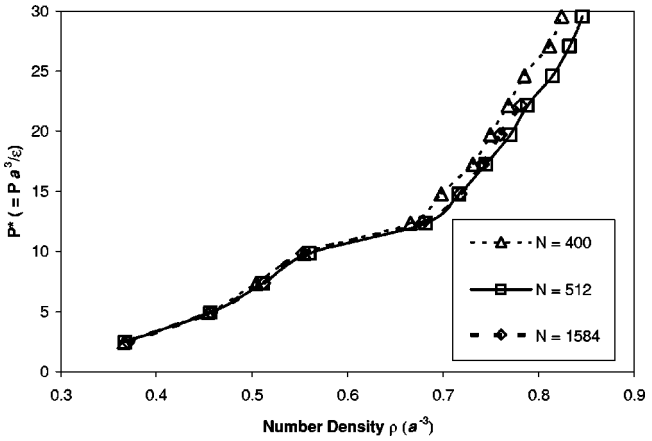

FIG. 10. Comparison of the equation-of-state curves from compression runs for a system of hard cuboids with $N=400$ (squares), $N=512$ (triangles), and $N=1584$ (solid circles). Lines are drawn to guide the eye. The error bars (standard deviation around average values) are smaller than the data symbols.

in these phases, the results shown may not be fully representative as they tend to exhibit large, long-period fluctuations during a run.

For the cubatic and crystal phases in the $N=512$ system, the shape of the box varies little from the original cubic shape despite the anisotropic volume moves used. Figure 10 shows the simulated equation-of-state curve from compression runs for the $N=400$ particle system, a size not commensurate with the perfect cubic arrangement of the particles in a cubic box. The purpose of these runs was to test if such an incommensurability could suppress or shift the isotropic–cubatic phase transition. Clearly, the isotropic–cubatic transition point and the isotropic branch are identical to those of the $N=512$ system. Although the cubatic and crystal phase branches are still apparent, for any given pressure, the densities for these phases in the $N=400$ system are consistently lower, the deviations being especially pronounced for the crystal-phase branch. This occurs because the perfect crystal arrangement is frustrated by the box dimensions in the $N=400$ system. Although the shape of the simulation box changed from its original cubic shape to try to accommodate a crystalline phase, box anisotropy cannot easily compensate for a lack of commensurability. In fact, a defect-free, close-packed cubic phase can only inhabit an orthorhombic box if the lengths of the box sides are multiples of the cubic-particle length; if those multiples are i_1, i_2, and i_3, then it must be true that $N=i_1\times i_2\times i_3$. For $N=400$, the most symmetric box for which the above condition is satisfied is $i_1:i_2:i_3=5:8:10$, which is a very large distortion for an originally cubic box, considering the sluggishness of volume deformation moves at high densities. In our simulations, the box shape was trapped at proportions around 7:7:8, probably because $7\times7\times8=392$ is very close to 400, but this necessarily leads to less efficient packing and lower densities. These effects are less important for the cubatic phase, so deviations between the $N=400$ and $N=512$ systems are mild and only become significant as the transition to the crystal phase is approached. As shown in Fig. 10, compression runs for a larger $N=1584$ system (also incommensurate in that $N^{1/3}\neq$ integer) give results for the isotropic and cubatic phases and their transition which agree very well with those reported for the $N=512$ system.

Compression simulation runs for smaller systems with $N=64$ and $N=216$ gave equation-of-state curves consistent with that from the expansion runs with the $N=512$ system. In the larger systems, the density at which the transitions take place increases slightly. In the smaller systems, the crystal phase was observed to form more readily upon compression and have a denser packing than that from the compression of the $N=512$ system; expectedly, the periodic boundary conditions tend to reinforce interparticle correlations when these become long ranged. As the system size increases, the compression route may lead to cubatic structures that then tunnel into imperfect crystal structures. At such high densities, partial and perfectly ordered states are likely to be separated by large free-energy barriers. The local Monte Carlo moves used here for configurational sampling are nonergodic in the crystal phase and could thus lead to kinetic trapping (particularly so if $N^{1/3}\neq$ integer). A more detailed study would be necessary to map out the free-energy landscape of the crystalline phase and determine the structure corresponding to the global minimum.

IV. CONCLUSIONS

In this work, Monte Carlo simulations were used to determine the bulk phase behavior of hard cuboidal particles. It was found that as the particle concentration is increased, three distinct phases form: an isotropic phase, a cubatic phase, and a crystalline phase. The isotropic–cubatic phase transition is first order and its location in the pressure–density diagram was readily determined. In contrast, the nature and location of the cubatic–crystal phase transition and the equilibrium structure of the crystal phase could not be determined accurately given the ergodic trapping associated with systems at high densities. The focus of this work was the prediction of the cubatic phase which has never been observed experimentally. In such a phase, the cuboid axes are aligned along three orthogonal directions but, unlike the crystal cubic phase, significant translational disorder is allowed. This cubatic phase thus constitutes a new example of an entropy-driven liquid-crystalline phase wherein ordering allows the cuboids to pack more efficiently and increase the volume accessible to them; the associated increase in translational entropy offsets the loss in orientational entropy.

A cubic or orthorhombic shape of the simulation box is arguably an appropriate choice to simulate our system where phases with cubic or near cubic symmetry are expected. This is absolutely true for the crystal phase. However, it is also conceivable that artificial boundary effects enhance (or even create) the cubatic phase. Our simulations revealed that the cubatic phase densities at the isotropic–cubatic and cubatic–crystal transitions are only very slightly changed with system size, and given that such transitions are quite distant from each other, it seems unlikely that the cubatic region would

disappear or even shrink significantly when $N \to \infty$. Further, results for the $N=400$ and $N=1584$ systems show that the isotropic–cubatic phase was not affected when the system size and box shape were incommensurate with respect to a cubic lattice arrangement. We speculate that simulations for the cubatic phase that allow for rhombohedral box shapes[19] (i.e., equal edges intersecting at oblique angles) will tend to orthorhombic shapes upon equilibration. Simulations in a box geometry that more closely mimics isotropic conditions—e.g., a truncated octahedron box[20]—would help confirm our estimate for the onset of the cubatic phase region; efforts along these lines are currently under way.

This work represents a first step in a combined simulation and experimental program aimed at elucidating the phase behavior of cuboidal particles in the bulk and in confined environments. It is envisioned that the cubatic phase detected in simulations, if realized experimentally, could exhibit unusual thermodynamic, optical, and rheological properties leading to potentially useful applications involving nanocomposites, electronic devices, and lubricants. Future studies will focus on elucidating how the onset and stability of cubatic (and possibly biaxial) liquid-crystalline phases is affected by experimentally relevant factors such as irregularities in shape (e.g., dull versus sharp edges, differences in side lengths, and size polydispersity) and the strength of the solvent-induced depletion interactions (e.g., due to the presence of nonadsorbing polymers in solution).

ACKNOWLEDGMENTS

The authors are grateful for financial support from the Cornell Center for Materials Research (CCMR) under the SEED program. CCMR is funded by the National Science Foundation.

[1] D. Frenkel, Physica A **313**, 1 (2002).
[2] P. Bolhuis, Ph.D. thesis, FOM-Institute for Atomic and Molecular Physics, 1996.
[3] C. Vega, C. McBride, and L. G. MacDowell, J. Chem. Phys. **115**, 4203 (2001).
[4] F. Escobedo, J. Chem. Phys. **118**, 10 262 (2003).
[5] Y. Sun and Y. Xia, Science **298**, 2176 (2002).
[6] A. Stroobants, H. N. W. Lekkerkerker, and D. Frenkel, Phys. Rev. Lett. **57**, 1452 (1986).
[7] P. Bolhuis and D. Frenkel, J. Chem. Phys. **106**, 666 (1997).
[8] P. J. Camp and M. P. Allen, J. Chem. Phys. **106**, 6681 (1997).
[9] R. Eppenga and D. Frenkel, Mol. Phys. **52**, 1303 (1984).
[10] M. A. Bates and D. Frenkel, Phys. Rev. E **57**, 4824 (1998).
[11] J. A. C. Veerman and D. Frenkel, Phys. Rev. A **45**, 5632 (1992).
[12] R. Blaak, D. Frenkel, and B. M. Mulder, J. Chem. Phys. **110**, 11652 (1999).
[13] D. Frenkel, in *Liquids, Freezing and the Glass Transition*, edited by J. P. Hansen, D. Levesque, and J. Zinn-Justin (North-Holland, Amsterdam, 1991), pp. 689–762.
[14] R. Blaak and B. Mulder, Phys. Rev. E **58**, 5873 (1998).
[15] M. Djikstra, D. Frenkel, and J. P. Hansen, J. Chem. Phys. **101**, 3179 (1994).
[16] A. Buhot and W. Krauth, Phys. Rev. Lett. **80**, 3787 (1998).
[17] D. Frenkel and B. Smit, *Understanding Molecular Simulation. From Algorithms to Applications*, 2nd ed. (Academic, San Diego, 2002).
[18] M. P. Allen, Liq. Cryst. **8**, 499 (1990).
[19] A. Parrinello and A. Rahman, J. Appl. Phys. **52**, 7182 (1981).
[20] D. J. Adams, Chem. Phys. Lett. **62**, 329 (1979).